Terahertz-bandwidth switching of heralded single photons

Kupchak, Connor; Erskine, Jennifer; England, Duncan; Sussman, Benjamin

Publisher's version / Version de l'éditeur:
https://doi.org/10.1364/OL.44.001427
Optics Letters, 44, 6, p. 1427, 2019

Optics Letters

Terahertz-bandwidth switching of heralded single photons

Connor Kupchak,[1,2,†] Jennifer Erskine,[1,2,†] Duncan England,[1,*] and Benjamin Sussman[1,2,3]

[1]Department of Physics, University of Ottawa, Ottawa, Ontario K1N 6N5, Canada
[2]National Research Council of Canada, 100 Sussex Drive, Ottawa, Ontario K1A 0R6, Canada
[3]e-mail: ben.sussman@nrc-cnrc.gc.ca
*Corresponding author: duncan.england@nrc-cnrc.gc.ca

Received 22 January 2019; accepted 10 February 2019; posted 14 February 2019 (Doc. ID 357896); published 12 March 2019

Optically induced ultrafast switching of single photons is demonstrated by rotating the photon polarization via the Kerr effect in a commercially available single-mode fiber. A switching efficiency of 97% is achieved with a ∼1.7 ps switching time and signal-to-noise ratio of ∼800. Preservation of the single-photon properties is confirmed by measuring no significant increase in the second-order autocorrelation function $g^{(2)}(0)$. These values are attained with only nanojoule-level pump energies that are produced by a laser oscillator with 80 MHz repetition rate. The results highlight a simple device capable of both high-bandwidth operations and preservation of single-photon properties for applications in photonic quantum processing and ultrafast time-gating or switching.

https://doi.org/10.1364/OL.44.001427

The ability to quickly switch, gate, or reroute optical signals is a key component of a range of modern technologies including communications [1], biomedical imaging [2], microscopy [3], spectroscopy [4], and quantum optics [5]. Driven by the development of modern lasers, device bandwidths measured in THz and duty cycles in GHz are available. The speed of traditional electro-optical devices is no longer sufficient for many applications. By contrast, all-optical approaches, which use a secondary light field to actively induce a switching mechanism, are capable of superior performance [6–8], and many future technologies will rely on these techniques. Unlike electro-optic devices, the high intensity required for all-optical switching has the potential to introduce or generate unwanted photons into the switched channel. In this context, the development of all-optical switches that are simultaneously capable of high bandwidths, high duty cycles, and single-photon-level operation is emerging as an important challenge in a range of photonic disciplines.

This Letter introduces a nonlinear technique for high-speed switching of single photons based on polarization rotation via the optical Kerr effect in single-mode fiber (SMF). The method is straightforward to implement, is interferometrically stable, requires only 10 cm of conventional SMF, and utilizes a low-power commercial femtosecond pump oscillator. Crucially, due to group velocity difference, the pump sweeps through the signal and induces switching. The pulse sweeping allows pump powers to be kept below thresholds for parasitic nonlinear optical processes such as Raman scattering and self-phase modulation. The short fiber length means that unwanted polarization rotations, dispersion, and multiphoton nonlinear effects can be kept to a minimum. The system scores highly in all of the key metrics outlined above: switching speeds near 1 ps achieved with a duty cycle of 80 MHz, an efficiency in excess of 95%, and a noise floor of 10^{-4} photons per switching window.

The noise properties of the device at the single photon level are benchmarked by a second order autocorrelation of the switched photons of $g^{(2)}(0) \approx 0.01$, confirming the quantum properties of the light are maintained. We therefore expect the switch to find applications in numerous photonic quantum information schemes such as metropolitan-scale quantum teleportation [9], high-dimensional encoding [10], and converting qubits between different degrees of freedom [11]. Away from quantum optics, high-contrast switching of photon-level light fields can benefit high-bandwidth applications including spectroscopy [12] and microscopy [13]. In applications like these, we expect this technique to be complementary to existing techniques based on nonlinear-optical loop mirrors (NOLM) [10,14–16] and time-gating by sum-frequency generation (SFG) [17–20] by offering faster switching than NOLM and higher efficiencies than SFG. However, SFG necessarily changes the frequency of the photon, which may be undesirable for some applications.

Heralded single photons are generated by spontaneous four wave mixing (SFWM) in a polarization-maintaining fiber (PMF) [21]. After generation, the signal photons are coupled into the 10-cm-long SMF where switching is achieved by rotating the polarization of the signal photons through the optical Kerr effect. The Kerr effect is a nonlinear process whereby a pump field is used to induce birefringence in a medium with a $\chi^{(3)}$ nonlinearity. When the medium is situated between two crossed polarizers, the incoming photons can only be transmitted when their polarization is rotated by interaction with the pump pulse. This setup is referred to as an optical Kerr shutter [22]. The efficiency of the rotation η can be given by [23]

$$\eta = \sin^2(2\theta)\sin^2\left(\frac{\Delta\phi}{2}\right), \quad (1)$$

where θ is the angle between the pump and signal polarization, with the maximum switching efficiency occurring when $\theta = 45°$. The nonlinear phase shift $\Delta\phi$ is given by [24]

$$\Delta\phi = \frac{2\pi n_2}{\lambda_{\text{signal}}} \int_0^L I_p(T - d_w z)\mathrm{d}z, \quad (2)$$

where z is the propagation distance along the fiber of length L, n_2 is the nonlinear refractive index, and λ_{signal} is the wavelength of the signal photon. The intensity profile of the pump pulse I_p is expressed in reduced time in the frame moving with the signal pulse $T = t - z/v_{gs}$. In a dispersive medium, the pump and signal will experience temporal walk-off given by $d_w = v_{gp}^{-1} - v_{gs}^{-1}$, where v_{gp} and v_{gs} are the pump and signal group velocities, respectively. In many high-bandwidth applications, dispersion is an inconvenience, but here it is key to the success of our scheme; by appropriately timing the pump pulse, it completely walks through the signal photon inside of the fiber. This results in a near-uniform phase-shift across the temporal profile of the signal photon while also reducing pump energy requirements.

An experimental schematic is shown in Fig. 1. Both the pump and signal beams originate from an 80 MHz repetition rate Ti-sapphire laser that produces pulses of 12 nm bandwidth at a central wavelength of 800 nm. Part of the oscillator beam is split off by a nonpolarizing beamsplitter to pump the photon pair source. Spectral filters are used to control the bandwidth, and then ~33 mW of pump power is coupled through a bow-tie style, 2.5 cm long, PMF (Fibercore HB800) [25]. The photon pair source generates signal and idler pairs at wavelengths of 685 and 980 nm, respectively, through SFWM (see inset in Fig. 1). After the photon source, the signal and idler photons are separated on a dichroic mirror. The idler channel is subsequently coupled to an avalanche photodiode (APD) using a SMF and serves as a herald for our photon counts.

The remaining oscillator beam serves as our pump pulse. In order to limit any noise photons generated due to self-phase modulation, the pump pulse duration is lengthened using a pair of bandpass filters such that $\Delta\lambda_{\text{pump}} = 2.6$ nm. Further noise reduction is achieved by chirping the pump with 5 cm of SF69 glass. The pump pulse is temporally combined with the signal by a variable delay (τ_{pump}) and spatially combined using a second dichroic mirror. In order to attain the peak switching efficiency governed by Eq. (1), the pulse polarizations are set to horizontal and −45° (antidiagonal) for the pump and signal, respectively. Any phase changes due to transmission of the signal through the dichroic mirror are precompensated using a set of quarter- and half-waveplates ($\lambda/4$ and $\lambda/2$) before combination.

A 10 cm long SMF (Thorlabs S630-HP) is used as the Kerr medium. The signal and pump are focused together into the 3.5 μm core using a 10 mm achromatic lens. Typically we achieve fiber coupling efficiencies of 40% and 60% for the signal and pump beams, respectively. After propagation through the SMF, we project the signal photons on to a diagonal (switched) or antidiagonal (unswitched) polarization using a $\lambda/2$ and polarizing beamsplitter (PBS). Spectral filters remove the pump beam before the signal photons are coupled to an APD via SMF. Coupling losses from the SMF and pump filtering correspond to a total transmission efficiency of 37%. We note that single photons can be coupled to SMF with up to 97% efficiency [26], so these coupling losses could be greatly improved.

We characterize the technique by measuring the switching efficiency and noise statistics as a function of pump pulse energy. With zero delay between the pump and signal pulses, we adjust the energy of the pump pulse using a neutral density filter wheel (not shown in Fig. 1). From Fig. 2 we see that the efficiency continually increases to a maximum of 96% at 3.0 nJ and follows the dependence expected from Eq. (1). By blocking the signal photons we can also measure the noise characteristics. The noise grows nonlinearly to a maximum of 1.3×10^{-4} noise photons per pump pulse. This nonlinear dependence is characteristic of $\chi^{(3)}$ processes such as self-phase modulation, four-wave mixing, and coherent Raman scattering in fiber [27]. Nonlinear $\chi^{(3)}$ processes cause broadening of the pump pulse spectrum; photons created within the signal pulse bandwidth are the source of the noise.

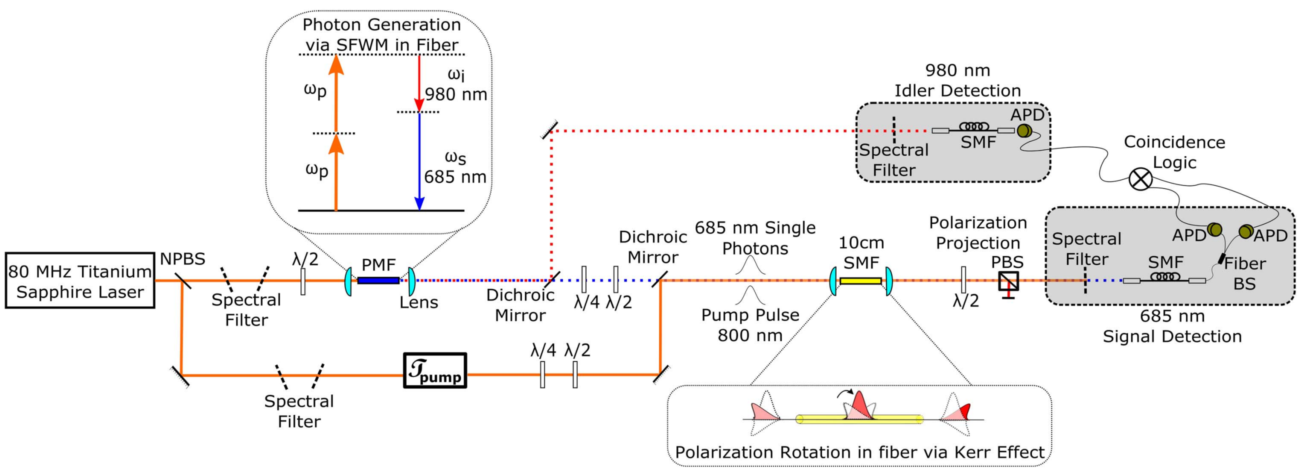

Fig. 1. Schematic diagram for the experimental setup. A SFWM process occurs inside the PMF to produce signal and idler photon pairs. Idler photons are used as a herald while signal photons undergo polarization rotation by the Kerr effect when temporally overlapped with a pump pulse (with variable delay τ_{pump}) inside a SMF (shown in bottom inset). Rotated signal photons can be measured on a single APD (not shown) for coincidence detection or split on a fiber beamsplitter (BS) and sent to independent APDs (as shown) in order to measure the single photon statistics. Corresponding optical components are described in the text.

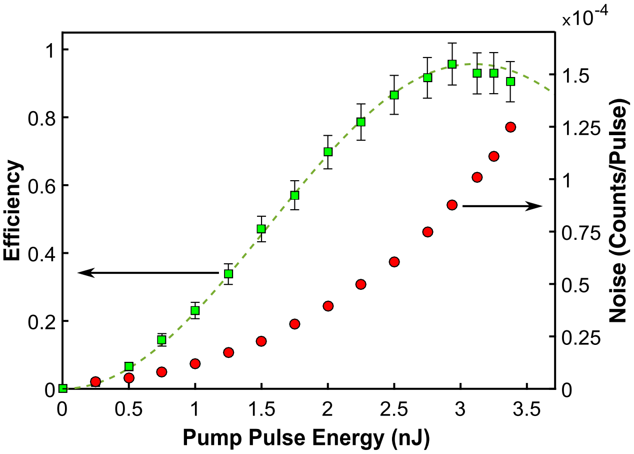

Fig. 2. Photon switching efficiency (left ordinate: green squares) with $\sin^2(\frac{\Delta\phi}{2})$ fit (dashed dark green line) and the noise counts per pulse (right ordinate: red circles) as a function of pump pulse energy. The pump energy is measured at the output of the SMF.

To evaluate the switching response, 3.0 nJ pump pulses are temporally delayed with respect to the signal photons via a motorized stage. The switched (diagonal) polarization projection is used to measure any photons successfully rotated in the Kerr medium and are only considered when coincident with a herald photon. Likewise, the "antiswitching" efficiency can also be evaluated by recording the absence of coincidences when the analysis optics are set to the unswitched projection.

Signal–idler coincidence counts in the switched and antiswitched polarizations are shown as a function of the pump temporal delay in Fig. 3. The maximum efficiency is found to be $\eta_{\rm switch} = 96.7 \pm 0.5\%$, calculated using the mean coincidence counts in the "flat-top" portion of the switched counts $N_{\rm switch}$. We define the efficiency as $\eta_{\rm switch} = (N_{\rm switch} - N_{\rm noise})/N_{\rm input}$. Here, N values refer to the mean coincidence counts for the case when the signal mode is switched $N_{\rm switch}$, blocked $N_{\rm noise}$, and passed through uncrossed polarizers in the absence of the pump $N_{\rm input}$. Similarly, the antiswitching efficiency calculated as $\eta_{\rm anti\text{-}switch} = 1 - (N_{\rm anti\text{-}switch} - N_{\rm noise})/N_{\rm input}$ yields a value of $\eta_{\rm anti\text{-}switch} = 98.0 \pm 0.3\%$. The small discrepancy in these two values is from the ~1% leakage of unswitched photons due to limitations of the polarization optics.

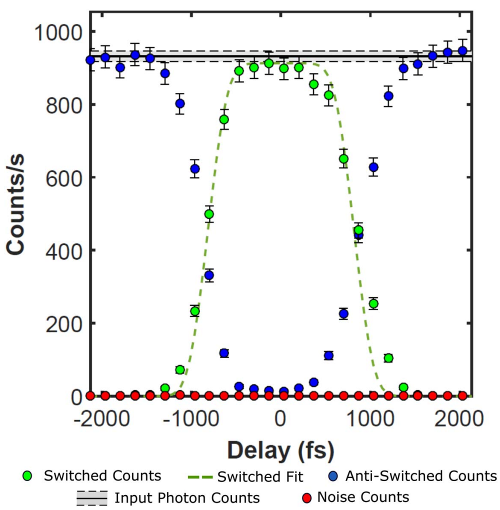

Fig. 3. Polarization switching (green circles) and antiswitching (blue circles) of the 685 nm signal photons when coincident with the 980 nm idler photons. The response of the switch is modeled using the pulse durations and the temporal walk-off between the pump and signal (dark green dashed line). Counts are shown relative to the input (nonrotated) photon count rate (solid line with shaded gray bar denoting uncertainty) and the noise counts due to the pump (red circles). The error bars are based on Poissonian statistics.

Here, the signal-to-noise ratio (SNR) is calculated to be $\mathrm{SNR} = N_{\rm switch}/N_{\rm noise} = 790 \pm 70$. Note that our SMF technique achieves a >80-fold increase in the SNR when compared to that found in a bulk crystal setup with an amplified pump [11]. This improvement can be attributed to a better spatial overlap supplied by the fiber and the lower pump energies.

We numerically evaluate Eq. (2) as a function of pump delay $\tau_{\rm pump}$ by considering the temporal profile of the pump pulse and the pump–signal walk-off. The pump pulse was measured by autocorrelation to be 410 fs, and the walk-off is calculated from the Sellmeier equation to be 1.6 ps. The resulting delay-dependent nonlinear phase shift $\Delta\phi(\tau_{\rm pump})$ is inserted into Eq. (1) to determine the intrinsic efficiency response function of the switch. This response function is independent of the switch input, and its width determines the fastest possible switching speed. To calculate the switching efficiency, we integrate the intrinsic response function over the duration of the signal photon, weighted by the temporal profile of the signal photon. The temporal profile of the input photons is estimated to be 390 fs. This total efficiency curve (green dashed line in Fig. 3) has a width of $\Delta t_{\rm calc} = 1.63$ ps, in good agreement with the measured duration ($t_{\rm switch} = 1.69 \pm 0.02$ ps). The intrinsic switching speed is limited by the length of the fiber and by the need for the pump and signal pulse to completely walk through each other. Faster switching speeds could be achieved with shorter fibers and pump pulses, but the minimum pump duration will remain limited due to self-phase modulation. The switch speed approaches the THz regime, but the maximum repetition rate will likely be ~GHz due to thermal effects in the fiber.

To examine how the switch affects the nonclassical properties of the single photons, we measure the heralded second order autocorrelation at zero time delay $g^{(2)}_{\rm switched}(0)$ of the switched signal photons. For this measurement we send the polarization rotated photons to a 50:50 fiber beamsplitter (Fig. 1), with each exit port coupled to independent APDs. The $g^{(2)}_{\rm switched}(0)$ value of the heralded SFWM source can be calculated by [28]

$$g^{(2)}_{\rm switched}(0) = \frac{P_{1,2,\rm i}}{P_{1,\rm i}P_{2,\rm i}}, \tag{3}$$

where $P_{1,2,\rm i}$ is the probability of a three-fold coincidence between the idler and both signal detectors, and $P_{1,\rm i}$ and $P_{2,\rm i}$ are the probabilities of a two-fold coincidence between the idler and signal detector 1, and the idler and signal detector 2, respectively.

Figure 4 shows the value of the second-order autocorrelation function of the heralded, switched photons $g^{(2)}_{\rm switched}(0)$ for increasing pump pulse energies. The input signal photons demonstrate good statistical properties, with $g^{(2)}_{\rm input}(0) = 0.0076 \pm 0.0003$, and the switched photons show only a modest increase in the measured $g^{(2)}_{\rm switched}(0)$. The increase in the second order

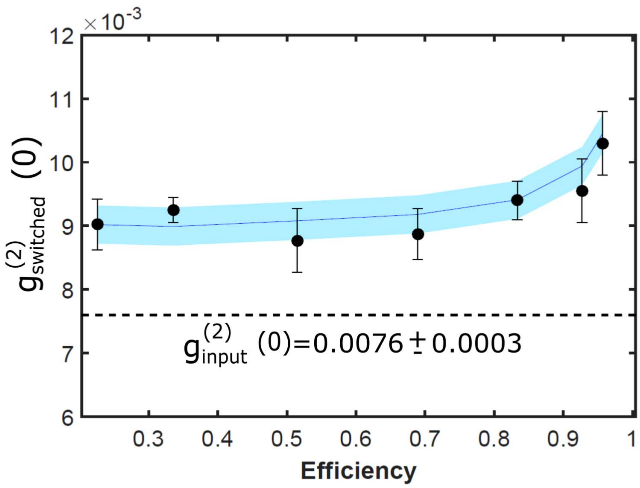

Fig. 4. Second-order correlation function $g^{(2)}_{\mathrm{switched}}(0)$ of the heralded, switched signal photons (filled circles) compared to that of the input signal photons (dashed line). The increase in the autocorrelation value of the switched photons can be modeled by considering the noise counts (blue line with shaded region denoting the uncertainty).

autocorrelation function can be explained by modeling the measured switched signal as an incoherent mixture of input signal and noise photons [29] and calculating the resulting expected autocorrelation according to

$$g^{(2)}_{\mathrm{expected}}(0) = \frac{N^2_{\mathrm{s,i}} g^{(2)}_{\mathrm{input}}(0) + 2N_{\mathrm{s,i}}N_{\mathrm{noise,i}} + N^2_{\mathrm{noise,i}} g^{(2)}_{\mathrm{noise}}(0)}{(N_{\mathrm{s,i}} + N_{\mathrm{noise,i}})^2}. \tag{4}$$

Here, $g^{(2)}_{\mathrm{input}}(0)$ is the measured heralded autocorrelation of the input photons, $N_{\mathrm{s,i}}$ is the number of heralded signal photons, $g^{(2)}_{\mathrm{noise}}(0)$ is the second order autocorrelation of the noise photons, and $N_{\mathrm{noise,i}}$ is the number of heralded noise photons. The second-order autocorrelation of the noise photons was measured to be $g^{(2)}_{\mathrm{noise}}(0) = 1.07 \pm 0.05$. From Fig. 4, we can see that this incoherent model closely matches the data.

In summary, we demonstrate single photon switching at picosecond timescales using a commercially available SMF and pump oscillator. The method achieves high efficiency, high duty-cycle, and excellent SNR values; requires only nanojoule pump energies; and preserves nonclassical single-photon statistics. Additionally, the pump energy requirements are within reach of commercial fiber oscillators, offering the opportunity for a completely integrated switch. The technique provides wavelength flexibility and can also perform all-optical phase-shifts. We expect this tool to find use in multiple quantum optical processing applications such as the conversion of photonic qubits [11], optical computing in a single spatial mode [30], and the processing of high-dimensional and hyperentangled quantum states [10,31]. Further applications include optical time-gating in wavelength restricted applications; the Kerr switch offers an alternative to the commonly used SFG approach [17,20] and can provide timing selectivity in applications beyond quantum protocols like spectroscopy [12] and microscopy [13].

Funding. Natural Sciences and Engineering Research Council of Canada (NSERC); National Research Council (NRC).

Acknowledgment. The authors are grateful for assistance from Khabat Heshami, Rune Lausten, Denis Guay, Doug Moffat, and Philip Bustard.

†These authors contributed equally to this work.

REFERENCES

1. S. Matsuo, A. Shinya, T. Kakitsuka, K. Nozaki, T. Segawa, T. Sato, Y. Kawaguchi, and M. Notomi, Nat. Photonics **4**, 648 (2010).
2. S. Andersson-Engels, R. Berg, S. Svanberg, and O. Jarlman, Opt. Lett. **15**, 1179 (1990).
3. G. Vicidomini, G. Moneron, K. Y. Han, V. Westphal, H. Ta, M. Reuss, J. Engelhardt, C. Eggeling, and S. W. Hell, Nat. Methods **8**, 571 (2011).
4. P. Matousek, M. Towrie, A. Stanley, and A. W. Parker, Appl. Spectrosc. **53**, 1485 (1999).
5. R. Prevedel, P. Walther, F. Tiefenbacher, P. Bohi, R. Kaltenbaek, T. Jennewein, and A. Zeilinger, Nature **445**, 65 (2007).
6. S. Friberg, Y. Silberberg, M. Oliver, M. Andrejco, M. Saifi, and P. Smith, Appl. Phys. Lett. **51**, 1135 (1987).
7. V. R. Almeida, C. A. Barrios, R. R. Panepucci, and M. Lipson, Nature **431**, 1081 (2004).
8. K. Nozaki, T. Tanabe, A. Shinya, S. Matsuo, T. Sato, H. Taniyama, and M. Notomi, Nat. Photonics **4**, 477 (2010).
9. R. Valivarthi, M. G. Puigibert, Q. Zhou, G. H. Aguilar, V. B. Verma, F. Marsili, M. D. Shaw, S. W. Nam, D. Oblak, and W. Tittel, Nat. Photonics **10**, 676 (2016).
10. M. A. Hall, J. B. Altepeter, and P. Kumar, Phys. Rev. Lett. **106**, 053901 (2011).
11. C. Kupchak, P. J. Bustard, K. Heshami, J. Erskine, M. Spanner, D. G. England, and B. J. Sussman, Phys. Rev. A **96**, 053812 (2017).
12. J. Takeda, K. Nakajima, S. Kurita, S. Tomimoto, S. Saito, and T. Suemoto, Phys. Rev. B **62**, 10083 (2000).
13. J. C. Blake, J. Nieto-Pescador, Z. Li, and L. Gundlach, Opt. Lett. **41**, 2462 (2016).
14. M. A. Hall, J. B. Altepeter, and P. Kumar, New J. Phys. **13**, 105004 (2011).
15. S. J. Nowierski, N. N. Oza, P. Kumar, and G. S. Kanter, Phys. Rev. A **94**, 042328 (2016).
16. N. N. Oza, Y.-P. Huang, and P. Kumar, IEEE Photon. Technol. Lett. **26**, 356 (2014).
17. J. M. Donohue, M. Agnew, J. Lavoie, and K. J. Resch, Phys. Rev. Lett. **111**, 153602 (2013).
18. J. M. Donohue, J. Lavoie, and K. J. Resch, Phys. Rev. Lett. **113**, 163602 (2014).
19. M. Allgaier, G. Vigh, V. Ansari, C. Eigner, V. Quiring, R. Ricken, B. Brecht, and C. Silberhorn, Quantum Sci. Technol. **2**, 034012 (2017).
20. J.-P. W. MacLean, J. M. Donohue, and K. J. Resch, Phys. Rev. Lett. **120**, 053601 (2018).
21. B. Smith, J. P. Mahou, O. Cohen, J. S. Lundeen, and I. A. Walmsley, Opt. Express **17**, 23589 (2009).
22. J. Etchepare, G. Grillon, R. Muller, and A. Orszag, Opt. Commun. **34**, 269 (1980).
23. H. Kanbara, H. Kobayashi, T. Kaino, T. Kurihara, N. Ooba, and K. Kubodera, J. Opt. Soc. Am. B **11**, 2216 (1994).
24. G. Agrawal, *Applications of Nonlinear Fiber Optics* (Academic, 2001).
25. J. Erskine, D. England, C. Kupchak, and B. Sussman, Opt. Lett. **43**, 907 (2018).
26. H. S. Zhong, Y. Li, W. Li, L. C. Peng, Z. E. Su, Y. Hu, Y. M. He, X. Ding, W. Zhang, H. Li, and L. Zhang, Phys. Rev. Lett. **121**, 250505 (2018).
27. A. M. Weiner, *Ultrafast Optics* (Wiley, 2009).
28. P. Grangier, G. Roger, and A. Aspect, Europhys. Lett. **1**, 173 (1986).
29. P. S. Michelberger, T. F. M. Champion, M. R. Sprague, K. T. Kaczmarek, M. Barbieri, X. M. Jin, D. G. England, W. S. Kolthammer, D. J. Saunders, J. Nunn, and I. A. Walmsley, New J. Phys. **17**, 043006 (2015).
30. P. C. Humphreys, B. J. Metcalf, J. B. Spring, M. Moore, X.-M. Jin, M. Barbieri, W. S. Kolthammer, and I. A. Walmsley, Phys. Rev. Lett. **111**, 150501 (2013).
31. T. Ikuta and H. Takesue, New J. Phys. **19**, 013039 (2017).